

Structures and Thermodynamics of Alzheimer's Amyloid- β A β (16–35) Monomer and Dimer by Replica Exchange Molecular Dynamics Simulations: Implication for Full-Length A β Fibrillation

Yasmine Chebaro,[†] Normand Mousseau,[‡] and Philippe Derreumaux^{*,†}

Laboratoire de Biochimie Théorique, UPR 9080 CNRS, Institut de Biologie Physico Chimique et Université Paris Diderot - Paris 7, 13 rue Pierre et Marie Curie, 75005 Paris, France, and Département de physique and Regroupement québécois sur les matériaux de pointe, Université de Montréal, C.P. 6128, succ. centre-ville, Montréal (Québec), Canada

Received: January 15, 2009; Revised Manuscript Received: April 6, 2009

Many proteins display a strand-loop-strand motif in their amyloid fibrillar states. For instance, the amyloid β -protein, A β 1–40, associated with Alzheimer's disease, displays a loop at positions 22–28 in its amyloid fibril state. It has been suggested that this loop could appear early in the aggregation process, but quantitative information regarding its presence in small oligomers remains scant. Because residues 1–15 are disordered in A β 1–42 fibrils and A β 10–35 forms fibrils in vitro, we select the peptide A β 16–35, centered on residues 22–28 and determine the structures and thermodynamics of the monomer and dimer using coarse-grained implicit solvent replica exchange molecular dynamics simulations. Our simulations totalling 5 μ s for the monomer and 12 μ s for the dimer show no sign of strong secondary structure signals in both instances and the significant impact of dimerization on the global structure of A β 16–35. They reveal however that the loop 22–28 acts as a quasi-independent unit in both species. The loop structure ensemble we report in A β 16–35 monomer and dimer has high similarity to the loop formed by the A β 21–30 peptide in solution and, to a lesser extent, to the loop found in A β 1–40 fibrils. We discuss the implications of our findings on the assembly of full-length A β .

1. Introduction

Self-assembly of the amyloid- β protein (A β) with 39–43 amino acids is frequently described by a nucleation-condensation mechanism where various oligomeric species are in dynamic equilibrium until the formation of a nucleus.¹ These early soluble intermediates are not simply building blocks leading to the fibrils, and there is substantial evidence that some of them rather than the mature insoluble amyloid fibrils are the most cytotoxic species in Alzheimer's disease.^{2,3}

The full-length A β 1–40/1–42 monomer is well-characterized by NMR spectroscopy in aqueous solution and we know that it is highly disordered, with a weak β -strand signal observed in the regions 17–21 and 31–36 and weak turn- or bendlike structures detected at positions 20–26.⁴ Limited proteolysis coupled to mass spectrometry further suggests that the amino acids 21–30 are protease-resistant.^{5,6}

In contrast to A β monomer, higher-order species, such as dimer⁷ and dodecamer,⁸ are not amenable to X-ray crystallography and solution state NMR spectroscopy, so that only low low-resolution information is available for these structures. For instance, circular dichroism (CD) of low molecular weight A β 1–40 gives 88% of random coil and β -turn and 12% of β -strand at 295 K, pH 7.5, and day 0;⁹ secondary composition for each individual oligomer remains to be determined.

Irrespective of the nature of the nucleus, dimers are the first step in A β assembly and toxicity that can disrupt cognitive

function and deserve, as such, serious quantitative analysis.³ While the free-energy landscape has been calculated for oligomers of small peptides (with less than \sim 8 amino acids)^{10–13} and the monomer of A β 1–28,¹⁴ A β 10–35,¹⁵ and A β 1–42,^{16,17} this information for A β 1–40/42 dimers is hampered by the slow convergence to equilibrium ensemble in explicit solvent.^{18,19} To accelerate convergence, one often resorts to coarse-grained proteins or all-atom models with implicit solvent.^{20–23} However, care must be taken to assess the validity of the simplification. Such a coarse-grained protein study was used for A β 1–42 dimer with discontinuous molecular dynamics simulations and a square-well force field, but none of the predicted planar β -sheet dimers were found stable in explicit solvent.²⁰ Jang and Shin studied the dimerization and tetramerization of A β 10–35 using all-atom replica exchange molecular dynamics (REMD) simulations with a Generalized Born (GB) solvent model,²¹ but their topologies have an averaged β -sheet content of 40% versus an experimental CD value of 0% for A β 1–40 dimers/tetramers.²⁴ We have also used an implicit solvent coarse-grained approach, the OPEP model coupled to REMD simulations, to study the dimer of A β 1–42 starting from Tycko's fibrillar model.²⁵ However, the 32-replica simulations with 120 ns at each temperature may be insufficiently long to ensure convergence,²³ a problem illustrated recently by all-atom REMD of three 17-residue peptides in implicit solvent, using 16 replicas for 200 ns²⁶ and OPEP-REMD simulations of various sequences.²⁷

Here we revisit A β monomer and dimer by applying the REMD-OPEP approach to the shorter A β 16–35 fragment. Four bodies of data justify this fragment in addition to the convergence problem. First, the residues 1–12 and 1–15 are disordered in the NMR-derived fibrillar models of A β 1–40²⁵ and

* To whom correspondence should be addressed. E-mail: Philippe.Derreumaux@ibpc.fr. Tel: 33 1 58 41 51 72. Fax: 33 1 58 41 50 26.

[†] Institut de Biologie Physico Chimique et Université Paris Diderot.

[‡] Université de Montréal.

A β 1–42,²⁸ respectively. Second, deletion of amino acids 1–9 and 36–42 does not prevent the truncated A β 10–35 peptide from forming fibrils with parallel β -sheets as in full-length A β fibrils.^{29,30} Third, A β 16–35 of sequence KLVFFA-EDVGSNKG-AIIGLM with two hydrophobic patches separated by a hydrophilic and charged region 22–29 (in italics) matches recent in vitro experiments indicating that hydrophobic stretches rather than specific side chains are sufficient to promote A β 42 fibril formation.³¹ Finally, A β 1–40 features a β -hairpin at positions 17–36 and an undetermined signal for the residues 1–15 and 37–40 when bound to the phage-display selected affibody ZA β 3.³²

By limiting our A β to the amino acids displaying a strand-loop-strand motif in A β 1–40/42 fibrils or in the A β 1–40 peptide bound to ZA β 3, we can focus on its probability within a dimer, a problem of fundamental importance as the strand-loop-strand is shared by several proteins in their fibrillar states,^{25,33,34} including the second WW domain of CA150³⁵ and the fragment 20–41 of β 2-microglobulin.³⁶ In addition, NMR studies on A β monomers report a loop signal at positions 20–26⁴ or 22–28.³⁷ This signal is often but not systematically supported by theoretical studies on the monomer of A β 1–35^{15,38} and A β 1–42.^{16,17} Whether it can be extrapolated to the dimer is unknown and is one of the goals of the present study.

2. Material and Methods

Coarse-Grained Model. OPEP is a generic force field for protein folding^{39–42} and aggregation,^{43–47} where all N, C α , C, O and H main-chain atoms are considered and each side-chain (Sc) is represented by a bead with appropriate van der Waals radius and geometry. The implicit solvent OPEP function is expressed as a sum of short-range (bond-lengths, bond angles, improper torsions of the side-chains and the amide bonds, backbone torsions), van der Waals (between all particles), and two-body and four-body hydrogen-bonding interactions.⁴⁸

Though OPEP averages out many fast degrees of motion,⁴⁹ the 3.2 parameter set used here performs well in discriminating native from non-native protein structures⁴⁸ and recovers (when coupled to REMD simulations) the proper thermodynamics and structures of the second 16-residue β -hairpin of protein G and the 20-residue Trp-cage peptide (within 1–2 Å from experiments).²⁷ REMD-OPEP simulations on a preformed six-chain A β 16–22 bilayer with four copies of an *N*-methylated A β 16–22 inhibitor also point to an interaction mechanism redirecting β -sheet oligomers into unstructured oligomers,⁵⁰ in agreement with biochemical and NMR studies on the interaction of α -synuclein with an inhibitor.⁵¹ Finally, we proposed from REMD-OPEP of A β 1–42 dimer that the impact of the lactam bridge is to increase the β -strand character of residues 17–21 and stabilize amyloid competent interactions between the residues 17–21 and Met35.⁵² This was confirmed by recent all-atom MD simulations of A β 10–35 in explicit solvent.⁵³

Simulations and Analyses. We have described the details of the REMD-OPEP protocol elsewhere.²⁷ Here, the N- and C-termini of A β 16–35 are neutralized by acetyl and NH₂ groups, respectively. REMD simulations are carried out at neutral pH as done experimentally,²⁹ using a logarithmic-like *T*-distribution with 20 replicas between 190 and 570 K: 190, 200, 214.5, 230, 246.7, 254, 264.6, 270, 283.8, 293, 304.4, 326.4, 350.1, 375.5, 402.7, 431.9, 463.2, 496.8, 533, and 571 K. All replicas are simulated at the desired temperature using the Berendsen's thermostat with a coupling constant of 0.5 ps and an integration time-step of 1 fs.⁴¹ Exchanges between replicas adjacent in temperature are attempted every 5.0 ps

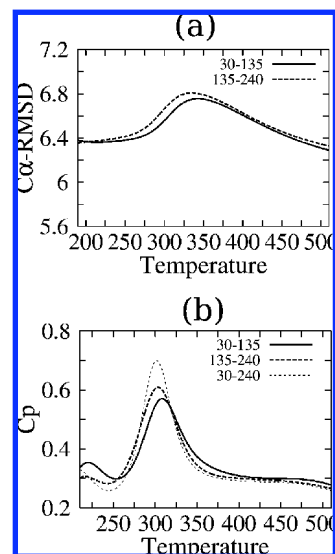


Figure 1. Structural properties of A β 16–35 monomer. (a) rmsd in Å as a function of temperature with respect to the structure of cluster C3 at 293 K shown in Figure 4: full line 30–135 ns and dashed line 135–240 ns. (b) Evolution of the specific heat (in kcal/(K·mol)) as a function of temperature: full line 30–135 ns, dashed line 135–240 ns, and gray dashed line 30–240 ns.

leading to an acceptance ratio of 30–40%. Production runs are performed in an open space for the monomer and in a sphere of 60 Å (leading to a concentration of \sim 40 μ M) with reflecting boundary conditions for the dimer.

For analysis, we exclude the first 30 and 100 ns of the monomer and dimer trajectories, respectively. For each chain, we compute the end-to-end distance between the Lys16 and Met35 C α atoms, and the C α or Sc distances between (Glu22 and Asp23) and Lys28. We also monitor the C α root-mean square deviation (rmsd) between selected conformations, and the secondary structure content of the equilibrium ensemble using the STRIDE program.⁵⁴ Two side-chains *k* and *l* are considered to be in contact if they deviate by less than 6.5 Å, and the conformations are clustered using a C α rmsd cutoff of 2 Å for the monomer and 3 Å for the dimer as described in ref 55. Thermodynamical information was determined using PT-WHAM.²⁷

3. Results

3.1. A β 16–35 Monomeric Structure Is Coil- and Turn-like. The A β 16–35 equilibrium structures in aqueous solution are determined using 20 replicas, each of 240 ns, starting from a randomly chosen state. Averaging separately over two time intervals, 30–135 ns and 135–240 ns, we can ensure that the simulation is well-converged and is properly sampling the equilibrium ensemble.

The *T*-plot of the C α -rmsd (Figure 1a) with respect to the C3 structure and of the heat capacity (Figure 1b) superpose very well between the two time intervals, with a small 4 K shift of the heat capacity peak. C3, corresponding to the predicted cluster of highest β -sheet content at 293 K, is characterized by a β -hairpin with two β -strands spanning Phe19-Ala21 and Gly29-Ile31. Overall, both panels indicate that the system is equilibrated over the full 30–240 ns interval. Using this time window, we find a well-defined heat capacity peak and a melting temperature T_m at 304 K. To identify the nature of the phase change, we now analyze successively the structural properties below and above T_m .

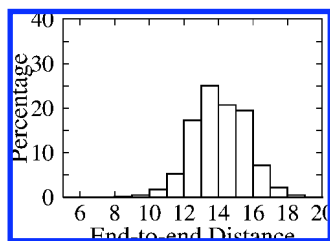


Figure 2. Distribution of the C α end-to-end distance of A β 16–35 monomer (in Å) at 293 K.

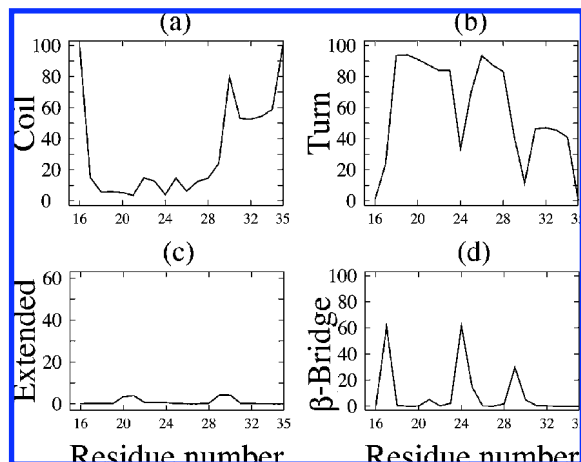


Figure 3. Secondary Structure Profiles of A β 16–35 monomer at 293 K.

Below T_m , at 293 K the end-to-end distance distribution is rather well-defined with 82% of the conformations within 12 and 16 Å (Figure 2). The percentage of coil, turn, β -strand and β -bridge as a function of the amino acid index in Figure 3 indicates that the monomer has no strong secondary structure. With minor populations, we find a β -sheet signal at positions 20–21 (probability of 4%) and 29–30 (4%), and a α -helix signal spanning the region 22–27 (0.4%, data not shown). Collectively our secondary structure description at 293 K with (58, 27%) of (turn, coil) and a weak β -strand signal at Leu17–Ala21 is consistent with our current NMR knowledge of the A β 10–35,⁵⁶ A β 1–40, and A β 1–42⁴ monomers in aqueous solution.

Using a 2.0 Å rmsd cutoff, all conformations at 293 K are grouped into 56 clusters. With a population of 63 and 29%, respectively, two dominant clusters emerge, C1 and C2. Figure 4 shows the center of these clusters as well as that of cluster C3 (population of 0.1%). The side-chain side-chain (Sc–Sc) probability contact maps of C1–C3 are also shown in Figure 4. C1 and C2, which deviate by 5.3 Å rms from each other, do not display any α -helix and β -sheet signal and are fully disordered. Nonetheless, they are stabilized by Sc–Sc hydrophobic interactions between the N-terminal residues Leu17–Phe20 and the C-terminal residues Ile31–Met35 as well as hydrophilic interactions between Glu22–Lys28 and Asp23–Lys28. Averaged over all conformations at 293 K, the Sc–Sc contacts between Glu22 and Lys28 and between Asp23 and Lys28 are found to be formed (distance of less than 6.5 Å) 61 and 80% of the time, respectively.

Above T_m , as should be expected, the number of clusters increases significantly (158 at 350 K vs 56 at 293 K), but the transition is characterized by a small change in secondary structure. We find that the (turn, coil) percentage is (60, 31%) at 350 K versus (58, 27%) at 293 K. Instead, the phase change

is associated with a reduced lifetime for salt bridges, the contact probability between Glu22 and Lys28 and between Asp23 and Lys28 decreasing to 38 and 57% at 350 K, respectively and the stabilization of a coil–turn C2-like structure (population of 70%).

To quantify further the transition, we calculate, using the residues 22–28, the rms deviation between our ensemble of structures and three reference states. These include the two NMR structures of the fragment A β 21–30 in solution determined by Teplow et al., referred here to as ab1 and ab2,⁵ and the solid-state NMR-derived A β 40 fibrillar model proposed by Tycko et al.,²⁵ referred here to as s-NMR. As shown in Figure 5, the rmsd distribution with respect to ab1 displays a peak at 1.0–1.5 Å (population of 55%) at 293 K, while it is rather uniform between 1.0 and 3.0 Å at 350 K. Note that our equilibrium ensemble shares less resemblance with ab2 and s-NMR at both T . This indicates that the peak in A β 15–35 heat capacity at 304 K corresponds essentially to a transition of the region 22–28 from the ab1 state to a more disordered state. The propensity of residues 22–28 for ab1 is however not fully lost at 350 K, but only 21% of the conformations deviate from ab1 with a rmsd <1.5 Å at 350 K versus 61% at 293 K.

Overall, the present propensity of the amino acids 22–28 to be structured in A β 15–35 as in the A β 21–30 peptide alone is fully consistent with all-atom REMD analyses of the monomer of A β 10–35 in explicit solvent,¹⁵ and the monomer A β 1–40/42 using GB solvent.¹⁷ This finding is also consistent with the protease-resistant character of the region 21–30 in the monomer of A β 1–40/42.^{5,6} Whether this region 22–28 can be considered as a folding independent unit in A β 40/42 aggregation, as suggested from monomer simulations,^{15,17} can be addressed by the dimer simulations.

3.2. A β 16–35 Dimers Display Little β -Sheet and α -Helical Contents. To determine how A β 16–35 structural and thermodynamical properties change upon dimerization, we launch a REMD simulation with 20 replicas, each of 600 ns, starting from a random dimeric structure shown in Figure 6a.

In Figure 6, we also show the variation of the total energy (panel b) and the end-to-end distance of chain 1 (panel c) as a function of T using the two independent intervals 100–350 ns and 350–600 ns. Note that the C α rmsd matrix between the 20 structures at times 100 and 350 ns leads to an averaged rmsd value of 7.4 Å and thus a high structural dissimilarity between the starting structures. Overall, the curves superpose well although there is a shift toward lower energies at most temperatures with longer simulation times, caused by an increased probability to find low energy states with time. To determine the impact of this energetic deviation on the structures, we plot in Figure 6d the percentage of turn as a function of the amino acids at 304 K using both intervals. We clearly see that the turn profiles averaged over both time intervals are very similar, demonstrating good convergence of our REMD simulations. Averaged over 100–600 ns, the heat capacity profile as a function of T in Figure 7 shows a well-defined peak at $T_m = 284$ K.

To clarify the phase change observed at 284 K, we first analyze the secondary structures profiles in Figure 8 at 270 K (< T_m) and 304 K (> T_m). We note that the turn, coil and β -bridge profiles as a function of the amino acid index are very similar at 270 and 304 K, and the main change is associated with a decrease in the β -strand content of the region Val18–Ala21 from an averaged value of 30 to 14% and of the region Gly29–Ile31 from 25 to 10%. Overall, the conformational ensemble of the A β 16–35 dimer shows 89% of coil–turn and 11% of β -strand

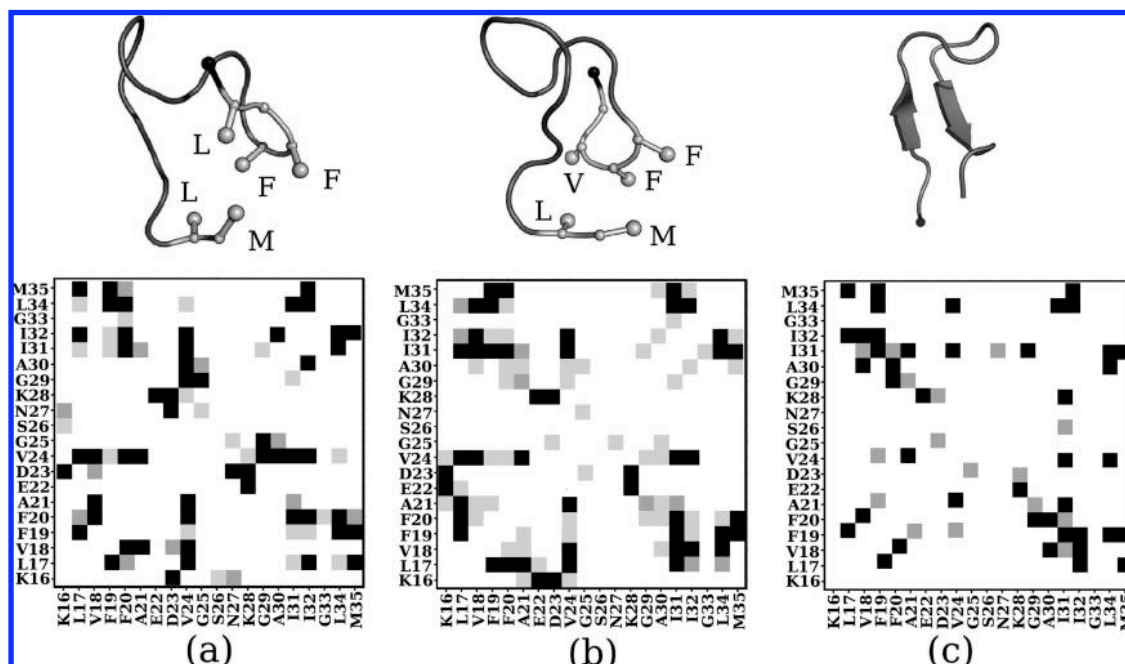


Figure 4. The C1–C3 monomeric clusters at 293 K and their corresponding side-chain–side-chain contact map probabilities. Probabilities are calculated using all structures belonging to each cluster. (a) C1 with the side-chain positions of L17, F19, F20, L34 and M35 indicated by gray balls; (b) C2 with the side-chain positions of V18, F19, F20, L34 and M35 indicated by gray balls; (c) C3 with a β -sheet spanning F19–A21 and G29–I31. Black balls represent the C α of K16. Black squares indicate a contact probability of 0.65–1, dark gray of 0.33–0.65 and light gray of 0.1–0.33.

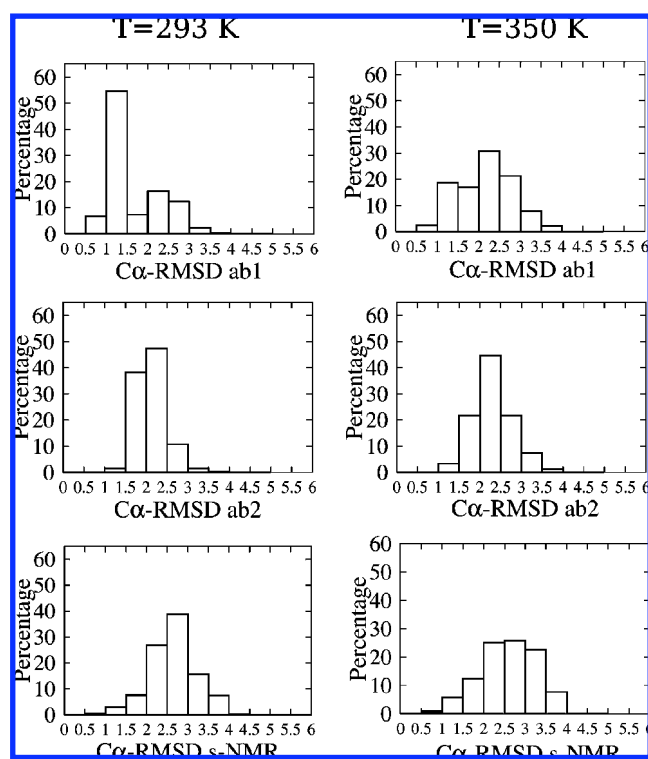


Figure 5. The C α -rmsd (in Å) of residues 22–28 in A β 16–35 monomer at 293 and 350 K with respect to the two liquid NMR structures of A β 21–30 (ab1 and ab2), and the fibril model of A β 1–40 (s-NMR).

at 270 K. We find it interesting that the A β 15–35 dimer shows almost no sign of α -helical and β -sheet structures consistent with CD spectroscopy results on A β 40 dimers/tetramers.²⁴ Furthermore, the first hydrophobic patch, VFF, is predicted to have a much higher propensity for β -sheet than the second hydrophobic patch, IIGLM. This is consistent with many

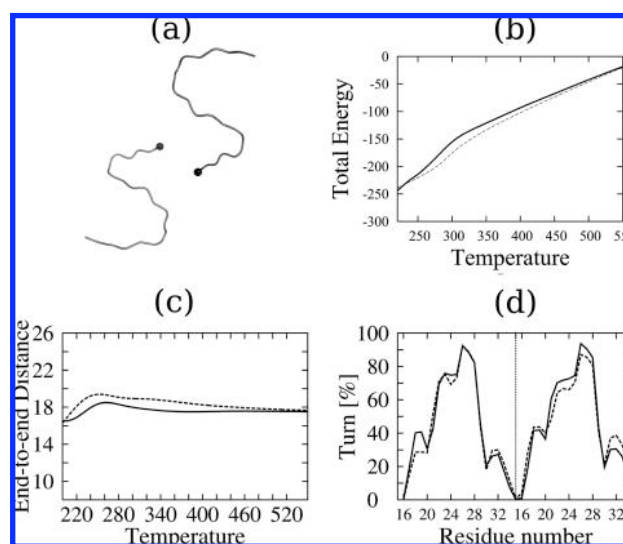


Figure 6. Structural and thermodynamical properties of A β 16–35 dimer. (a) Starting dimeric structure. The black balls represent the C α of K16. (b) Evolution of the total energy (in kcal/mol) as a function of temperature: full line using 100–350 ns and dashed line using 350–600 ns. (c) Evolution of the C α end-to-end distance (in Å) of chain 1 as a function of temperature using 100–350 ns (solid line) or 350–600 ns (dashed line). (d) Percentage of turn as a function of the residue number in both chains at 304 K using 100–350 ns (solid line) and 350–600 ns (dashed line). The dashed vertical line separates the two chains.

experimental studies indicating that the region 16–22 plays a critical role in full-length A β assembly and is an important binding site for blocking fibrillogenesis.

The transition at 284 K can also be described by comparing the centers of the dominant clusters as a function of temperature. Here, we cluster all structures between 100 and 600 ns using a 3 Å C α -rmsd cutoff. Figure 9 reports the center of the two most populated clusters and of the cluster with the highest β -sheet content at $T_1 = 270$ K and at two temperatures above T_m , $T_2 =$

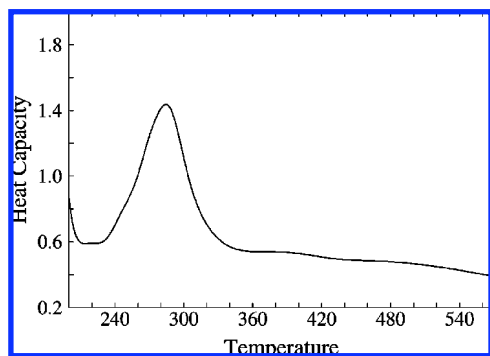


Figure 7. $A\beta_{16-35}$ dimer: evolution of the specific heat (in kcal/(K·mol)) as a function of temperature using the 100–600 ns interval.

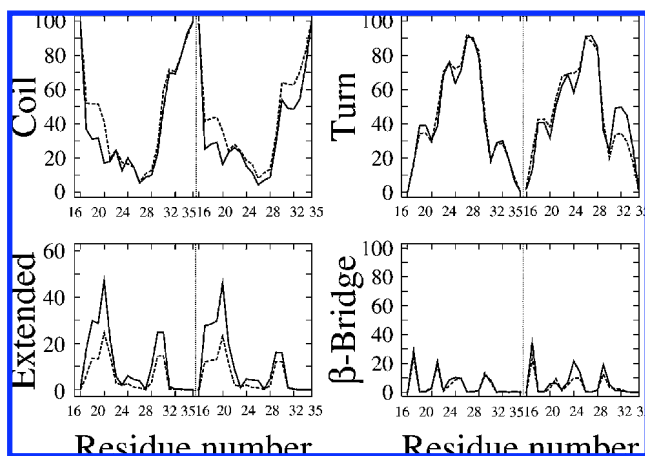


Figure 8. Secondary structure profiles of $A\beta_{16-35}$ dimer at 270 K (solid line) and 304 K (dashed line). The dashed vertical line separates the two chains.

293 K and $T_3 = 304$ K. The side-chain side-chain contact maps of the most populated cluster at 270 and 293 K are shown in Figure 10.

We note that for the three temperatures, the two largest clusters include 59, 47, and 48% of all conformations. Comparing the two dominant clusters at 270 and 293 K in Figure 9, we see that the transition is characterized by a conversion of a dimer with a small antiparallel β -sheet spanning Val18-Ala21 (in chain 1) and Leu17-Phe20 (in chain 2) into a disordered dimer with parallel orientation of the N-terminal regions. In both instances, the two C-terminal regions have a propensity to be parallel to each other. The random coil character of the dimer above T_m is further illustrated at 304 K, where the two dominant states are free of any β -sheet structure. We also find that at lower temperatures one chain forms a β -hairpin spanning Phe20-Ala21 and Gly29-Ala30, and at all temperatures the dimer has a probability of less than 1.5% to display highly ordered β -sheet structures. At 270 and 293 K, these β -rich structures consist of β -strands at positions Leu17-Glu22 (chain 1), Lys16-Ala21 (chain 2), and Gly29-Ile31 (chain 1), and therefore no β signal in the second hydrophobic IIGLM patch. Figure 10 also shows that the dominant cluster at 273 K is stabilized by more hydrophobic interactions involving the N- and C-terminal regions of both chains than the dominant cluster at 293 K.

The dimer equilibrium ensemble differs substantially from the parallel β -sheet organization of NMR-derived fibrillar models. This result provides strong evidence that the dimer of $A\beta_{16-35}$ must reorganize extensively en route to amyloid fibril formation in agreement with dimer simulations on $A\beta_{1-28}$ ⁵⁵ and $A\beta_{1-42}$ ²³ and fluorescence quenching analysis of $A\beta_{40}$.⁷

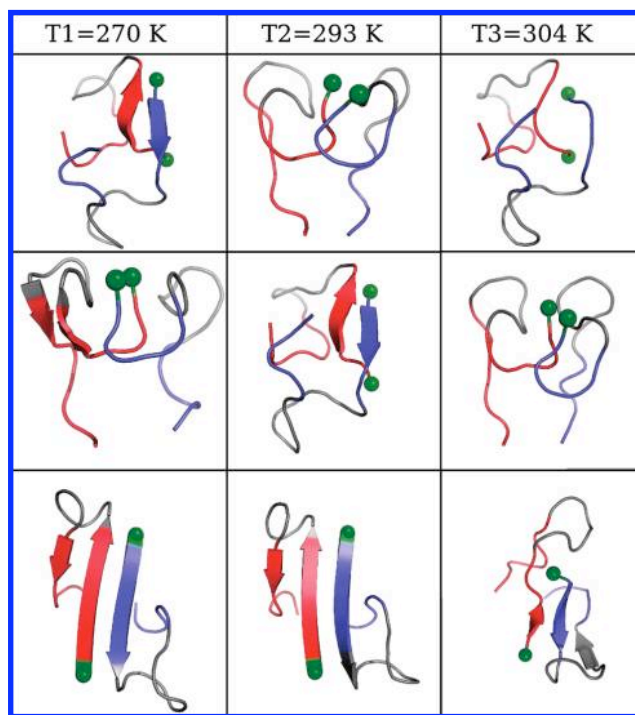


Figure 9. Centers of $A\beta_{16-35}$ dimeric clusters using a $C\alpha$ -rmsd cutoff of 3 Å at $T_1 = 270$ K, $T_2 = 293$ K, and $T_3 = 304$ K. (top) The most populated cluster; (middle) the second most populated cluster; (bottom) the cluster with the highest β -sheet content. The populations of the clusters are respectively 33.1, 26.3, and 24.5% for the first clusters, 26.4, 20.7, and 23.3% for the second clusters, and 0.8, 0.15, and 1.4% for the β -sheet clusters. Chain 1 is in red, chain 2 is in blue, except the region 22–28 in gray, and the $C\alpha$ of Lys-16 are represented by green balls.

3.3. The Monomer and Dimer of $A\beta_{15-35}$ Share Common and Different Properties. As a first step toward comparing the properties shared by $A\beta_{15-35}$ in the monomer and the dimer, it is important to note that the two chains in the dimer adopt similar but not identical conformational ensembles. Asymmetry is seen in comparing the secondary structure profiles of chains 1 and 2 (Figure 8) and is further supported by the distinct number of clusters for each chain as a function of T in Table 1. Asymmetric properties were already discussed in dimer simulations of $A\beta_{10-35}$ ⁵⁷ and $A\beta_{9-40/9-42}$ ¹⁸ and whether they help understand the polymorphism of amyloid fibrils remains to be determined.

First, dimerization impacts the thermodynamics of the system and unfolding occurs at lower temperatures in the dimer. We find a decrease in T_m of 20 K from the monomer to the dimer, consistent with on-lattice Monte Carlo simulations of protein models.⁵⁸

Second, dimerization impacts the number of clusters in a temperature-dependent manner. In particular, we see that the number of clusters for either chain in the dimer, N_{cd} , and the number of clusters for the monomer, N_{cm} , are very similar for $T \leq T_m$, but N_{cd} is smaller at higher temperatures. For instance, at 270 K chain 1, chain 2, and the monomer display 26, 30, and 30 clusters, while at 326 K we have 68, 58, and 108 clusters, respectively.

Third, interchain interactions impact the global structures of $A\beta_{16-35}$. By calculating the rms deviation between the dominant clusters of the monomer and the dimer, we find no structural overlap between the dominant cluster of the monomer and the conformation of each chain in the two dominant clusters of the dimer with the rmsd never approaching 3 Å.

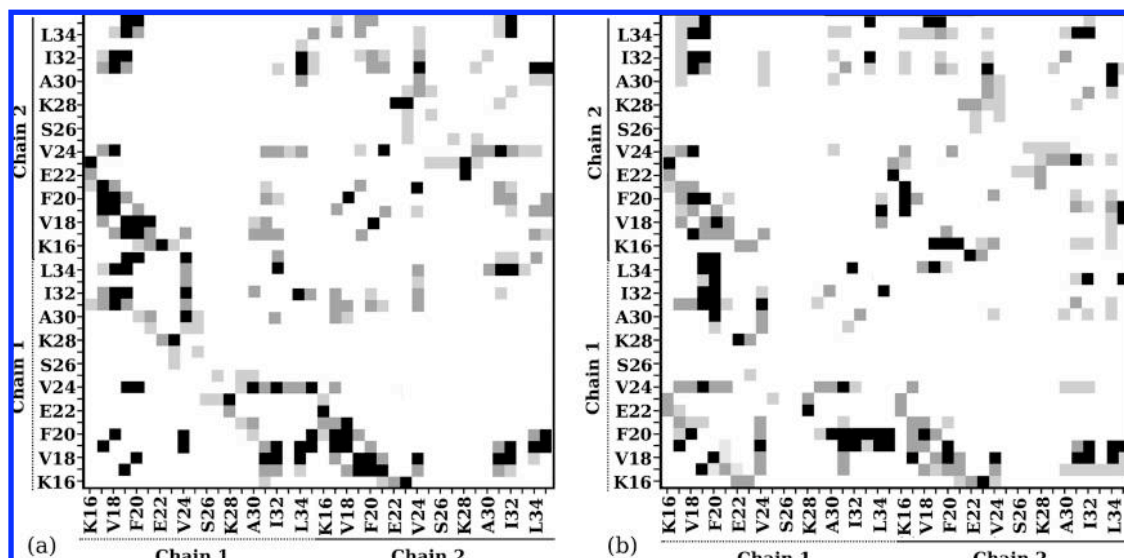


Figure 10. Side-chain–side-chain contact probability maps of A β 16–35 dimers. The centers of the most populated clusters at 270 K (a) and 293 K (b). Black squares indicate a contact probability of 0.65–1, dark gray of 0.33–0.65, and light gray of 0.1–0.33.

TABLE 1: Number of Clusters Using a C α -RMSD Cutoff Indicated in Parentheses

T (K)	254	264.6	270	283.8	293	304	326.5	350	375.5	402.7	431.9	463.3
monomer (2 Å)	20	22	30	43	56	71	108	158	235	333	542	737
dimer 2 chains (3 Å)	20	30	31	37	45	69	83	137	184	318	525	892
dimer chain 1 (2 Å)	18	24	26	27	30	43	68	151	181	266	430	647
dimer chain 2 (2 Å)	20	25	30	22	44	55	58	98	139	161	291	460

Interestingly, dimerization has a much reduced effect on the structures of region 22–28. This can be first determined by computing the formation probabilities of intramolecular salt bridges between Glu22 and Lys28 and between Asp23 and Lys28 at 270 K. Using a 6.5 Å cutoff, we find that within the dimer the intramolecular Sc22–Sc28 contact is formed 37 and 50% of the time in chains 1 and 2, the intramolecular Sc23–Sc28 contact is formed 57 and 64% of the time in chains 1 and 2, while both the intermolecular Sc22–Sc28 and Sc23–Sc28 contacts are formed 7% of the time averaging over both chains. Comparing with the lower temperature monomer populations, 61% for Sc22–Sc28 and 80% for Sc23–Sc28, the intramolecular populations Sc22–Sc28 and Sc23–Sc28 in the dimer are still substantial.

The reduced impact of dimerization on the loop ensemble is also demonstrated by the distribution of the rmsd deviations between the conformations of amino acids 22–28 in A β 16–35 dimer and the three ab1, ab2, and s-NMR reference states. As reported in the previous section, conformations of the region 22–28 in A β 16–35 monomer are much more similar to ab1 than to ab2 and s-NMR. As seen in Figure 11, the same picture emerges from the structures of region 22–28 in both chains of the dimer. We have \sim 20% of the conformations in chain 1 and 37% of the conformations in chain 2 deviating by less than 1.5 Å from ab1 (panels a and b). We also find that \sim 9 and 7% of the conformations in chains 1 and 2, respectively, deviate by less than 1.5 Å rmsd from s-NMR (panels e and f), that is, the conformation of the loop region within the A β 40 fibril, deviating by 2.4 Å rmsd from ab1.

4. Conclusions

Many proteins display a β -strand-loop- β -strand motif in their amyloid fibrillar states. For most amyloids, however, direct structural characterization of the nucleus is still out of reach using standard biology tools and the rate-limiting step of

A β 1–40/42 polymerization remains a matter of debate. Thus far, five events not mutually exclusive have been proposed to be rate-limiting: (a) the formation of the loop within region 21–30,^{5,59} (b) the formation of a multimeric β -sheet spanning residues 16–20,^{23,60} (c) an increase population of β -structure at positions 17–21,^{23,61} (d) a structural reorganization of the

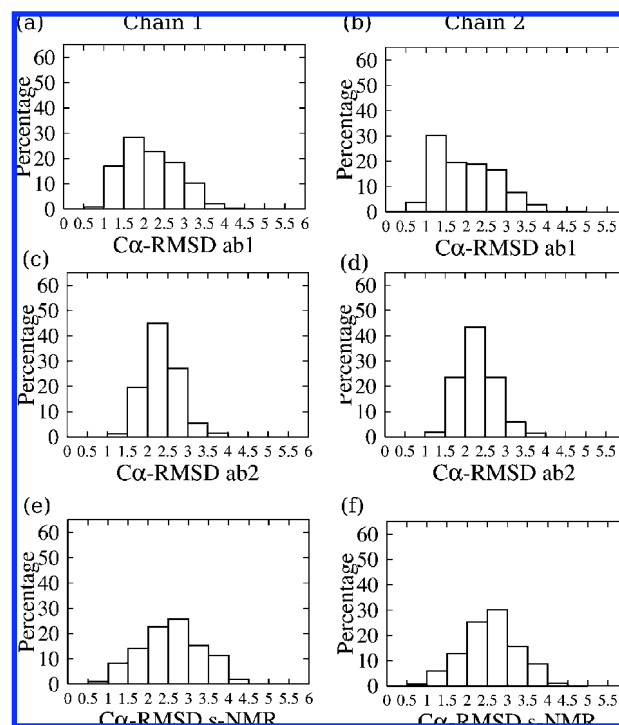


Figure 11. A β 16–35 dimer: C α -rmsd (in Å) of residues 22–28 in chains 1 and 2 at 293 K with respect to the two liquid NMR structures of A β 21–30 (ab1 and ab2), and the fibril model of A β 1–40 (s-NMR). Results for chain 1 are in panels a, c, and e.

monomer structure,^{6,55} and (e) the formation of a hairpinlike structure spanning 17–35.⁵³

Because the monomer/dimer transition is the first step in aggregation, we determine the monomeric and dimeric equilibrium ensembles of A β 16–35 using the OPEP coarse-grained protein force field coupled to replica exchange molecular dynamics. Although the generation of A β from the amyloid precursor through the action of secretases produces A β 1–40 and A β 1–42 peptides, other truncated A β variants, such as A β 11–40⁶² and A β 31–35⁶³ also produce disease-associated aggregates. These data along with the disorder of residues 1–15 and 37–40 in A β 1–40 monomer interacting with ZA β 3³² make the fragment A β 16–35 a good model to understand A β 1–40 assembly.¹⁹ The extrapolation of A β 16–35 to A β 1–42 is very reasonable for the loop 22–28 but is less evident for the populations of β -strands at positions 16–22 and 30–35. Indeed, the higher assembly rate in A β 42 than in A β 40 may result from an increase of contacts within the region 35–42 and between the regions 35–42 and 17–22 in the monomer.^{16,17,64} Overall, our findings can be summarized as follows.

First, the A β 16–35 monomer is dominantly turnlike and coil-like, but displays with a marginal probability a β -hairpin. This hairpin, recently described by all-atom MD of A β 10–35 with a lactam bridge,⁵³ is consistent with the structure adopted by A β 1–40 in interaction with the phage-display selected affibody ZA β 3,³² suggesting that the binding occurs with a configuration visited by A β 1–40 alone. At low temperature, the 22–28 loop is found to be similar to the A β 21–30 NMR solution structure,^{5,65,66} and is also conserved, with a lower population, at higher temperatures. Overall these findings are consistent with previous simulations of the monomer of A β 10–35¹⁵ and A β 1–40/42.^{17,64}

Second, interpeptide chains impact the global structure of A β 16–35, but have little effects on the 22–28 loop conformation. The loop structure ensemble we report in both monomer and dimer of A β 16–35 has high similarity to the loop formed by the A β 21–30 peptide in solution,^{5,66} and to a lesser extent, to the loop in A β 1–40 fibrils. We also find that dimerization populates equally the antiparallel and parallel orientations of the N-terminal regions 16–21 with little β -sheet structure, and leaves the C-terminal regions 31–35 unstructured and in parallel orientation. This topological and structural description on A β 16–35 in conjunction with dimer A β 1–42 simulations⁵² reinforces the idea that β -rich structures with fibril-like parallel sheets are marginally populated in a dimer of A β 1–40/1–42.

In summary, our results provide strong evidence that the loop 22–28 acts as a quasi-independent unit in both the monomer and dimer of A β 16–35. Whether this loop ensemble remains in higher-order assemblies of A β 16–35 has to be established, but this would simplify the structural identification of A β 1–40/1–42 cytotoxic species.

Acknowledgment. P.D. is supported by the Centre National de la Recherche Scientifique, the Université Paris Diderot - Paris 7, and the European Grant “ImmunoPrion, FP6-Food-023144, 2006–2009”. N.M. is supported in part by NSERC, FQRNT (Quebec), and the Canada Research Chair Foundation.

References and Notes

- Hardy, J. A.; Higgins, G. A. *Science* **1992**, *256* (5054), 184–185.
- Lambert, M. P.; Barlow, A. K.; Chromy, B. A.; Edwards, C.; Freed, R.; Liosatos, M.; Morgan, T. E.; Rozovsky, I.; Trommer, B.; Viola, K. L.; Wals, P.; Zhang, C.; Finch, C. E.; Krafft, G. A.; Klein, W. L. *Proc. Natl. Acad. Sci. U.S.A.* **1998**, *95* (11), 6448–6453.
- Cleary, J. P.; Walsh, D. M.; Hofmeister, J. J.; Shankar, G. M.; Kuskowski, M. A.; Selkoe, D. J.; Ashe, K. H. *Nat. Neurosci.* **2005**, *8* (1), 79–84.
- Hou, L.; Shao, H.; Zhang, Y.; Li, H.; Menon, N. K.; Neuhaus, E. B.; Brewer, J. M.; Byeon, I.-J. L.; Ray, D. G.; Vitek, M. P.; Iwashita, T.; Makula, R. A.; Przybyla, A. B.; Zagorski, M. G. *J. Am. Chem. Soc.* **2004**, *126* (7), 1992–2005.
- Lazo, N. D.; Grant, M. A.; Condrion, M. C.; Rigby, A. C.; Teplow, D. B. *Protein Sci.* **2005**, *14* (6), 1581–1596.
- Grant, M. A.; Lazo, N. D.; Lomakin, A.; Condrion, M. M.; Arai, H.; Yamin, G.; Rigby, A. C.; Teplow, D. B. *Proc. Natl. Acad. Sci. U.S.A.* **2007**, *104* (42), 16522–16527.
- Garzon-Rodriguez, W.; Vega, A.; Sepulveda-Becerra, M.; Milton, S.; Johnson, D. A.; Yatsimirsky, A. K.; Glabe, C. G. *J. Biol. Chem.* **2000**, *275* (30), 22645–22649.
- Lesné, S.; Koh, M. T.; Kotilinek, L.; Kaye, R.; Glabe, C. G.; Yang, A.; Gallagher, M.; Ashe, K. H. *Nature* **2006**, *440* (7082), 352–357.
- Kirkitadze, M. D.; Condrion, M. M.; Teplow, D. B. *J. Mol. Biol.* **2001**, *312* (5), 1103–1119.
- Meli, M.; Morra, G.; Colombo, G. *Biophys. J.* **2008**, *94* (11), 4414–4426.
- Irbäck, A.; Mitternacht, S. *Proteins* **2008**, *71* (1), 207–214.
- Strodel, B.; Whittleston, C. S.; Wales, D. J. *J. Am. Chem. Soc.* **2007**, *129* (51), 16005–16014.
- Song, W.; Wei, G.; Mousseau, N.; Derreumaux, P. *J. Phys. Chem. B* **2008**, *112* (14), 4410–4418.
- Khandogin, J.; Brooks, C. L. *Proc. Natl. Acad. Sci. U.S.A.* **2007**, *104* (43), 16880–16885.
- Baumketner, A.; Shea, J.-E. *J. Mol. Biol.* **2007**, *366* (1), 275–285.
- Sgourakis, N. G.; Yan, Y.; McCallum, S. A.; Wang, C.; Garcia, A. E. *J. Mol. Biol.* **2007**, *368* (5), 1448–1457.
- Yang, M.; Teplow, D. B. *J. Mol. Biol.* **2008**, *384* (2), 450–464.
- Huet, A.; Derreumaux, P. *Biophys. J.* **2006**, *91* (10), 3829–3840.
- Ma, B.; Nussinov, R. *Proc. Natl. Acad. Sci. U.S.A.* **2002**, *99* (22), 14126–14131.
- Urbanc, B.; Cruz, L.; Ding, F.; Sammond, D.; Khare, S.; Buldyrev, S. V.; Stanley, H. E.; Dokholyan, N. V. *Biophys. J.* **2004**, *87* (4), 2310–2321.
- Jang, S.; Shin, S. *J. Phys. Chem. B* **2008**, *112* (11), 3479–3484.
- Anand, P.; Nandel, F. S.; Hansmann, U. H. E. *J. Chem. Phys.* **2008**, *128* (16), 165102.
- Melquiond, A.; Dong, X.; Mousseau, N.; Derreumaux, P. *Curr. Alzheimer Res.* **2008**, *5* (3), 244–250.
- Huang, T. H.; Yang, D. S.; Plaskos, N. P.; Go, S.; Yip, C. M.; Fraser, P. E.; Chakrabarty, A. *J. Mol. Biol.* **2000**, *297* (1), 73–87.
- Petkova, A. T.; Yau, W.-M.; Tycko, R. *Biochemistry* **2006**, *45* (2), 498–512.
- Strodel, B.; Fitzpatrick, A. W.; Vendruscolo, M.; Dobson, C. M.; Wales, D. J. *J. Phys. Chem. B* **2008**, *112* (32), 9998–10004.
- Chebaro, Y.; Dong, X.; Laghaei, R.; Derreumaux, P.; Mousseau, N. *J. Phys. Chem. B* **2009**, *113* (1), 267–274.
- Lührs, T.; Ritter, C.; Adrian, M.; Rieck-Loher, D.; Bohrmann, B.; Döbeli, H.; Schubert, D.; Riek, R. *Proc. Natl. Acad. Sci. U.S.A.* **2005**, *102* (48), 17342–17347.
- Fraser, P. E.; McLachlan, D. R.; Surewicz, W. K.; Mizzen, C. A.; Snow, A. D.; Nguyen, J. T.; Kirschner, D. A. *J. Mol. Biol.* **1994**, *244* (1), 64–73.
- Benzinger, T. L.; Gregory, D. M.; Burkoth, T. S.; Miller-Auer, H.; Lynn, D. G.; Botto, R. E.; Meredith, S. C. *Proc. Natl. Acad. Sci. U.S.A.* **1998**, *95* (23), 13407–13412.
- Kim, W.; Hecht, M. H. *Proc. Natl. Acad. Sci. U.S.A.* **2006**, *103* (43), 15824–15829.
- Hoyer, W.; Grönwall, C.; Jonsson, A.; Stahl, S.; Härd, T. *Proc. Natl. Acad. Sci. U.S.A.* **2008**, *105* (13), 5099–5104.
- Croixmarie, V.; Briki, F.; David, G.; Coïc, Y.-M.; Ovtracht, L.; Doucet, J.; Jamin, N.; Sanson, A. *J. Struct. Biol.* **2005**, *150* (3), 284–299.
- Luca, S.; Yau, W.-M.; Leapman, R.; Tycko, R. *Biochemistry* **2007**, *46* (47), 13505–13522.
- Ferguson, N.; Becker, J.; Tidow, H.; Tremmel, S.; Sharpe, T. D.; Krause, G.; Flinders, J.; Petrovich, M.; Berriman, J.; Oschkinat, H.; Fersht, A. R. *Proc. Natl. Acad. Sci. U.S.A.* **2006**, *103* (44), 16248–16253.
- Liang, C.; Derreumaux, P.; Mousseau, N.; Wei, G. *Biophys. J.* **2008**, *95* (2), 510–517.
- Zhang, S.; Iwata, K.; Lachenmann, M. J.; Peng, J. W.; Li, S.; Stimson, E. R.; Lu, Y.; Felix, A. M.; Maggio, J. E.; Lee, J. P. *J. Struct. Biol.* **2000**, *130* (2–3), 130–141.
- Han, W.; Wu, Y.-D. *J. Am. Chem. Soc.* **2005**, *127* (44), 15408–15416.
- Derreumaux, P. *J. Chem. Phys.* **1999**, *111* (5), 2301–2310.
- Forcellino, F.; Derreumaux, P. *Proteins* **2001**, *45* (2), 159–166.
- Derreumaux, P.; Mousseau, N. *J. Chem. Phys.* **2007**, *126* (2), 025101.
- Derreumaux, P. *Biophys. J.* **2001**, *81* (3), 1657–1665.

- (43) Santini, S.; Wei, G.; Mousseau, N.; Derreumaux, P. *Structure* **2004**, *12* (7), 1245–1255.
- (44) Santini, S.; Mousseau, N.; Derreumaux, P. *J. Am. Chem. Soc.* **2004**, *126* (37), 11509–11516.
- (45) Mousseau, N.; Derreumaux, P. *Acc. Chem. Res.* **2005**, *38* (11), 885–891.
- (46) Melquiond, A.; Mousseau, N.; Derreumaux, P. *Proteins* **2006**, *65* (1), 180–191.
- (47) Melquiond, A.; Boucher, G.; Mousseau, N.; Derreumaux, P. *J. Chem. Phys.* **2005**, *122* (17), 174904.
- (48) Maupetit, J.; Tuffery, P.; Derreumaux, P. *Proteins* **2007**, *69* (2), 394–408.
- (49) Derreumaux, P.; Wilson, J.; Vergoten, G.; Peticolas, W. *J. Phys. Chem.* **1989**, *93*, 1338–1350.
- (50) Chebaro, Y.; Derreumaux, P. *Proteins* **2009**, *75*, 442–52.
- (51) Ehrnhoefer, D. E.; Bieschke, J.; Boeddrich, A.; Herbst, M.; Masino, L.; Lurz, R.; Engemann, S.; Pastore, A.; Wanker, E. E. *Nat. Struct. Mol. Biol.* **2008**, *15* (6), 558–566.
- (52) Melquiond, A.; Dong, X.; Mousseau, N.; Derreumaux, P. *Curr. Alzheimer Res.* **2008**, *5* (3), 244–250.
- (53) Reddy, G.; Straub, J. E.; Thirumalai, D. *J. Phys. Chem. B* **2009**, *113*, 1162–72.
- (54) Frishman, D.; Argos, P. *Proteins* **1995**, *23*, 566–579.
- (55) Dong, X.; Chen, W.; Mousseau, N.; Derreumaux, P. *J. Chem. Phys.* **2008**, *128* (12), 125108.
- (56) Lee, J. P.; Stimson, E. R.; Ghilardi, J. R.; Mantyh, P. W.; Lu, Y. A.; Felix, A. M.; Llanos, W.; Behbin, A.; Cummings, M.; Crieckinge, M. V. *Biochemistry* **1995**, *34* (15), 5191–5200.
- (57) Tarus, B.; Straub, J. E.; Thirumalai, D. *J. Mol. Biol.* **2005**, *345* (5), 1141–1156.
- (58) Cellmer, T.; Bratko, D.; Prausnitz, J. M.; Blanch, H. *Proc. Natl. Acad. Sci. U.S.A.* **2005**, *102* (33), 11692–11697.
- (59) Sciarretta, K. L.; Gordon, D. J.; Petkova, A. T.; Tycko, R.; Meredith, S. C. *Biochemistry* **2005**, *44* (16), 6003–6014.
- (60) Tjernberg, L. O.; Tjernberg, A.; Bark, N.; Shi, Y.; Ruzsicska, B. P.; Bu, Z.; Thyberg, J.; Callaway, D. J. E. *Biochem. J.* **2002**, *366* (Pt 1), 343–351.
- (61) Baumketner, A.; Krone, M. G.; Shea, J.-E. *Proc. Natl. Acad. Sci. U.S.A.* **2008**, *105* (16), 6027–6032.
- (62) Willem, M.; Dewachter, I.; Smyth, N.; Dooren, T. V.; Borghgraef, P.; Haass, C.; VanLeuven, F. *Am. J. Pathol.* **2004**, *165* (5), 1621–1631.
- (63) Wu, B.; Kitagawa, K.; Liu, B.; Zhang, N.; Xiong, Z.; Inagaki, C. *Neurosci. Lett.* **2006**, *396* (2), 148–152.
- (64) Lam, A. R.; Teplow, D. B.; Stanley, H. E.; Urbanc, B. *J. Am. Chem. Soc.* **2008**, *130* (51), 17413–17422.
- (65) Fawzi, N. L.; Phillips, A. H.; Ruscio, J. Z.; Doucleff, M.; Wemmer, D. E.; Head-Gordon, T. *J. Am. Chem. Soc.* **2008**, *130* (19), 6145–6158.
- (66) Chen, W.; Mousseau, N.; Derreumaux, P. *J. Chem. Phys.* **2006**, *125* (8), 084911.

JP900425E